

# Mechanical properties of twisted radio waves

H. Then

*Institute of Physics, University of Oldenburg, D-26111 Oldenburg, Germany*

Spin and orbital angular momentum densities are connected to helicity (circular polarization) and topological charge (azimuthal phase shift and vorticity). Computing the electromagnetic fields emitted by a circular antenna array, analytic expressions are found for the densities of energy, linear and angular momentum in terms of helicity and vorticity. In particular, it is found that the angular momentum density can be clearly separated into spin and orbital parts; a result that was previously known to be true in the paraxial approximation. Moreover, the approach via an antenna array illuminates light from a new perspective and complements previous studies of orbital angular momentum of electromagnetic waves. As a special case of the present approach, it is now for the first time possible to separate the angular momentum of an electric point dipole into its spin and its orbital part. Emerging as a byproduct, but being of deep interest in its own is the finding of radio waves associated to longitudinal currents. They have never been investigated until recently, nor their existence has even been appreciated.

PACS numbers: 03.50.De,42.50.Tx,41.20.Jb,07.57.-c

Keywords: classical electromagnetism, optical angular momentum, electromagnetic wave propagation, radio-wave instruments

## I. INTRODUCTION

Any interaction between radiation and matter is inevitably accompanied by an exchange of momentum. In addition to linear momentum, Poynting suggested that circularly polarized light should carry spin angular momentum [1] and Allen et al. proposed that it also carries orbital angular momentum [2]. In the past few decades the use of spin and orbital angular momentum has come to the fore in optics [3] and in atomic and molecular physics [4]. The orbital angular momentum of electromagnetic waves now takes an important position in various fields of research and applications, ranging from manipulating and orienting small particles [5], information-rich radio astronomy [6], novel wireless communication concepts [7], quantum entanglement [8], cryptography, and quantum computation [9]. Applications for the use of the orbital angular momentum of radio waves have been proposed in [10], including radio astronomy and space physics [11, 12, 13, 14, 15, 16, 17].

In the literature different views can be found concerning the possibility of separating the spin angular momentum, see [18, 19, 20]. In computing the electromagnetic fields emitted by a circular antenna array and expressing the angular momentum density explicitly in terms of helicity and vorticity, I find that the angular momentum of the emitted waves can be clearly separated into spin and orbital angular momentum; a result that was previously known in the paraxial approximation [21]. Crucial for the analytic computation is the fact that the radiated densities of energy, linear momentum, and angular momentum are homogeneous functions of distance. This allows to neglect the non-radiating terms. The only approximation made is in the geometrical setup by assuming an array of infinite many antennas.

## II. SETUP

The vector potential of a single or crossed electric dipole antenna that is in harmonic oscillation with frequency  $\omega$  can be expressed by  $\mathbf{A}(\mathbf{r}, t) = -\frac{\mu_0 d}{8\pi} \mathbf{I}(t) \frac{e^{ikr}}{r}$ , cf. Eqs. (9.16) and (9.27) in [22].  $i$  is the imaginary unit,  $k$  is the magnitude of the wave vector,  $\hat{\mathbf{r}} = \frac{\mathbf{r}}{r}$  is the unit vector in the direction of  $\mathbf{r}$ ,  $\mu_0$  is the magnetic permeability,  $d$  is the length of each dipole and  $\mathbf{I}$  is the antenna current.

Taking the potentials and fields to be complex valued, the harmonic time dependence is attributed by multiplying the antenna current with the appropriate complex factor,  $\mathbf{I}(t) = \mathbf{I}e^{-i\omega t}$ . The physical fields result from taking the real parts.

Placing  $N$  crossed dipole antennas on a circle at the positions

$$\mathbf{r}_n = \begin{pmatrix} R \cos(2\pi \frac{n}{N}) \\ R \sin(2\pi \frac{n}{N}) \\ 0 \end{pmatrix}, \quad n = 1 \dots N, \quad (1)$$

where  $R$  is the radius of the antenna array, see Fig. 1 (left), and feeding the antennas with the currents

$$\mathbf{I}_n = \frac{1}{\sqrt{2}} \begin{pmatrix} I \\ ihI \\ 0 \end{pmatrix} e^{2\pi il \frac{n}{N}}, \quad n = 1 \dots N, \quad (2)$$

see Fig. 1 (right), the total vector potential reads

$$\mathbf{A} = \frac{1}{\sqrt{2}} \begin{pmatrix} 1 \\ ih \\ 0 \end{pmatrix} \mathcal{A}(r) \mathcal{C}(\theta, \phi) \quad (3)$$

with  $\mathcal{A} = -\frac{I\mu_0 d}{8\pi} \frac{e^{ikr}}{r}$  and  $\mathcal{C} = \sum_{n=1}^N e^{2\pi il \frac{n}{N}} e^{-ik\hat{\mathbf{r}} \cdot \mathbf{r}_n}$ .  $I$  is the amplitude of the antenna currents,  $h = \pm 1$  is the helicity associated with circular polarization, and  $l \in \mathbb{Z}$  is

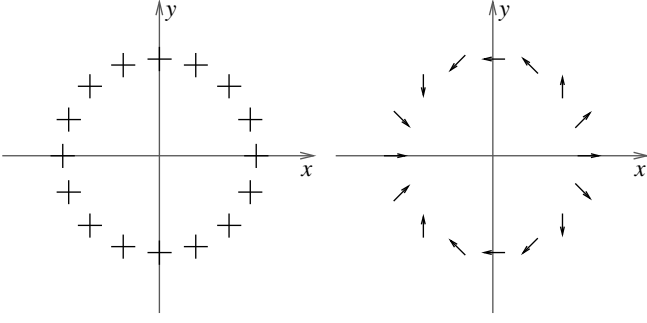


FIG. 1: Plots of the  $N$  crossed dipole antennas and their currents. The left panel displays the positions and orientations of the crossed dipole antennas, and the right panel displays the current vector at each crossed dipole for  $N = 16$ ,  $h = 1$ ,  $l = -2$ , and  $t = 0$ .

the topological charge. The topological charge attributes an azimuthal phase shift of  $\exp(2\pi i l n / N)$  to the antenna currents and is associated with vorticity.

If the number of antennas is sufficiently large, typically  $N = 16$  antennas are enough, the sum in  $\mathcal{C}$  can be approximated by a Riemann integral and expressed by its residuum,

$$\mathcal{C}(\theta, \phi) \simeq \frac{N}{2\pi} \int_0^{2\pi} d\Phi e^{i l \Phi} e^{-i k R \sin \theta \cos(\Phi - \phi)} \quad (4)$$

$$= e^{i l \phi} N \operatorname{Res}_{z=0} \frac{1}{l} e^{-i k R \sin \theta \cosh(\frac{1}{l} \ln z)}, \quad (5)$$

yielding  $\frac{\partial}{\partial \phi} \ln \mathcal{C} = i l$  and  $\frac{\partial}{\partial \theta} \ln \mathcal{C} = \text{real}$ . This implies  $\mathcal{C}^* \mathcal{C}$  to be independent of  $\phi$ .

### III. FIELDS

From the vector potential follows the magnetic field  $\mathbf{B} = \nabla \times \mathbf{A}$ . Separating the magnetic field into its far and its near field terms,  $\mathbf{B} = \mathbf{B}_{\text{far}} + \mathbf{B}_{\text{near}}$ , results in

$$\mathbf{B}_{\text{far}} = i k \hat{\mathbf{r}} \times \mathbf{A} \quad (6)$$

and

$$\mathbf{B}_{\text{near}} = e^{i k r} \nabla \times (\mathbf{A} e^{-i k r}), \quad (7)$$

where  $e^{-i k r} \mathbf{B}_{\text{far}}$  and  $e^{-i k r} \mathbf{B}_{\text{near}}$  are homogeneous functions in  $r$  of degree  $-1$  and  $-2$ , respectively.

The electric field outside of sources is given by  $\mathbf{E} = \frac{i c}{k} \nabla \times \mathbf{B}$ , where  $c$  is the speed of light. The electric field results in  $\mathbf{E} = \mathbf{E}_{\text{far}} + \mathbf{E}_{\text{inter}} + \mathbf{E}_{\text{near}}$  with

$$\mathbf{E}_{\text{far}} = i k c [\mathbf{A} - (\hat{\mathbf{r}} \cdot \mathbf{A}) \hat{\mathbf{r}}], \quad (8)$$

$$\mathbf{E}_{\text{inter}} = -c [\hat{\mathbf{r}} (\nabla \cdot (\mathbf{A} e^{-i k r})) + \nabla (\hat{\mathbf{r}} \cdot \mathbf{A} e^{-i k r})] e^{i k r}, \quad (9)$$

and

$$\mathbf{E}_{\text{near}} = \frac{i c}{k} [\nabla (\nabla \cdot (\mathbf{A} e^{-i k r})) - \nabla^2 (\mathbf{A} e^{-i k r})] e^{i k r}. \quad (10)$$

The individual terms of the electric field are called the far,  $\mathbf{E}_{\text{far}}$ , the intermediate,  $\mathbf{E}_{\text{inter}}$ , and the near electric field,  $\mathbf{E}_{\text{near}}$ . Apart from the complex phase, they are homogeneous functions in  $r$  of degree  $-1$ ,  $-2$ , and  $-3$ , respectively.

### IV. DENSITIES OF ENERGY AND MOMENTA

The energy density is defined by

$$w = \frac{\epsilon_0}{4} (\mathbf{E} \cdot \mathbf{E}^* + c^2 \mathbf{B} \cdot \mathbf{B}^*), \quad (11)$$

where  $\epsilon_0$  is the electric permittivity of free space.

The density of any conserved quantity  $Q$  that propagates radially with a constant speed is required to be homogeneous in  $r$  of degree  $-2$ . Imagine a set of spheres centered at the origin. If  $Q$  is conserved, the total flow of  $Q$  through the surfaces must be the same for each sphere. This is only possible if the  $r^2$  dependence of the surface area cancels with the  $r^{-2}$  dependence of the density of the conserved quantity.

For instance, the conservation law of energy imposes the condition that the radiated energy density is homogeneous in  $r$  of degree  $-2$  which is fulfilled by the leading order term of the energy density,

$$w_{\text{far}} = \frac{\epsilon_0}{4} (\mathbf{E}_{\text{far}} \cdot \mathbf{E}_{\text{far}}^* + c^2 \mathbf{B}_{\text{far}} \cdot \mathbf{B}_{\text{far}}^*). \quad (12)$$

The linear momentum density is given by the Poynting vector  $\mathbf{p} = \frac{\epsilon_0}{2} \Re[\mathbf{E} \times \mathbf{B}^*]$  which can be splitted into homogeneous functions in  $r$  of degree  $-2$ ,  $-3$ , and higher order terms,  $\mathbf{p} = \mathbf{p}_{\text{far}} + \mathbf{p}_{\text{next}} + \mathbf{p}_{\text{rest}}$  with

$$\mathbf{p}_{\text{far}} = \frac{\epsilon_0}{2} \Re[\mathbf{E}_{\text{far}} \times \mathbf{B}_{\text{far}}^*] \quad (13)$$

$$\mathbf{p}_{\text{next}} = \frac{\epsilon_0}{2} \Re[\mathbf{E}_{\text{far}} \times \mathbf{B}_{\text{near}}^* + \mathbf{E}_{\text{inter}} \times \mathbf{B}_{\text{far}}^*] \quad (14)$$

and  $\mathbf{p}_{\text{rest}} = O(1/r^4)$ . Due to the conservation of linear momentum, the radiated linear momentum density is given by the far field term,  $\mathbf{p}_{\text{far}}$ , only.

The angular momentum density is defined by  $\mathbf{j} = \mathbf{r} \times \mathbf{p}$ . Because of the conservation law of angular momentum the radiated angular momentum density is homogeneous in  $r$  of degree  $-2$ . This has important consequences. Namely, the pure far field does not contribute to the radiated angular momentum density, since  $\mathbf{r} \times \mathbf{p}_{\text{far}}$  would be a homogeneous function in  $r$  of degree  $-1$ . It is the next order term,  $\mathbf{j}_{\text{far}} = \mathbf{r} \times \mathbf{p}_{\text{next}}$ , that yields the radiated angular momentum density; in agreement with the fact that  $\mathbf{p}_{\text{far}}$  is parallel to  $\mathbf{r}$ .

Plugging the vector potential (3) into the expressions for the magnetic and electric fields and evaluating the radiated densities of energy, linear momentum, and angular momentum results in

$$w_{\text{far}} = \frac{k^2}{4\mu_0} \left( \frac{I\mu_0 d}{8\pi r} \right)^2 (1 + \cos^2 \theta) (\mathcal{C}^* \mathcal{C}), \quad (15)$$

$$\mathbf{p}_{\text{far}} = \frac{\hat{\mathbf{r}}k^2}{4c\mu_0} \left( \frac{I\mu_0 d}{8\pi r} \right)^2 (1 + \cos^2 \theta) (\mathcal{C}^* \mathcal{C}), \quad (16)$$

and

$$\mathbf{j}_{\text{far}} = \frac{-\hat{\theta}k}{4c\mu_0} \left( \frac{I\mu_0 d}{8\pi r} \right)^2 \left\{ h \left( 2 \sin \theta (\mathcal{C}^* \mathcal{C}) - \cos \theta \frac{\partial}{\partial \theta} (\mathcal{C}^* \mathcal{C}) \right) + l \frac{1 + \cos^2 \theta}{\sin \theta} (\mathcal{C}^* \mathcal{C}) \right\}, \quad (17)$$

where  $\hat{\mathbf{r}}$ ,  $\hat{\theta}$ , and  $\hat{\phi}$  are the unit vectors of spherical coordinates. Since the density of angular momentum scales with distance like  $r^{-2}$ , the angular momentum is transported all the way out to infinity; a fact that is not always well appreciated.

## V. SPIN AND ORBITAL ANGULAR MOMENTUM

Separating the angular momentum density in terms that depend on the topological charge  $l$  only and in terms that depend on the helicity  $h$ ,  $\mathbf{j}_{\text{far}} = \mathbf{l}_{\text{far}} + \mathbf{s}_{\text{far}}$ , allows to identify the topological charge (vorticity) with the orbital angular momentum,

$$\mathbf{l}_{\text{far}} = l \frac{-\hat{\theta}k^2}{4\omega\mu_0} \left( \frac{I\mu_0 d}{8\pi r} \right)^2 \left( \frac{1 + \cos^2 \theta}{\sin \theta} \right) (\mathcal{C}^* \mathcal{C}), \quad (18)$$

and the helicity (polarization) with the spin orbital angular momentum,

$$\mathbf{s}_{\text{far}} = h \frac{-\hat{\theta}k^2}{4\omega\mu_0} \left( \frac{I\mu_0 d}{8\pi r} \right)^2 \left( 2 \sin \theta (\mathcal{C}^* \mathcal{C}) - \cos \theta \frac{\partial}{\partial \theta} (\mathcal{C}^* \mathcal{C}) \right). \quad (19)$$

Surprisingly, the orbital angular momentum density is easier to describe than the density of the spin angular momentum. The density of the orbital angular momentum is completely independent of the helicity, but the spin angular momentum density depends via  $\mathcal{C}^* \mathcal{C}$  on the topological charge. If the topological charge vanishes,  $\mathcal{C}^* \mathcal{C}$  has its maximum at  $\theta = 0$ , while for any non-vanishing topological charge,  $\mathcal{C}^* \mathcal{C}$  vanishes at  $\theta = 0$ ,

$$(\mathcal{C}^* \mathcal{C})|_{\theta=0} = \begin{cases} N^2 & \text{if } l = 0, \\ 0 & \text{if } l \neq 0, \end{cases} \quad (20)$$

and  $\frac{\partial}{\partial \theta} (\mathcal{C}^* \mathcal{C})|_{\theta=0} = 0$ . Figure 2 shows graphs of  $\mathcal{C}^* \mathcal{C}$ . In all plots an array radius of  $R = 2\lambda$  is used, where  $\lambda = \frac{2\pi}{k}$  is the wavelength.

## VI. RADIATION PATTERNS

Radiation patterns of the energy are shown in Fig. 3. If the topological charge vanishes,  $l = 0$ , the circular antenna array emits a beam that has maximum intensity

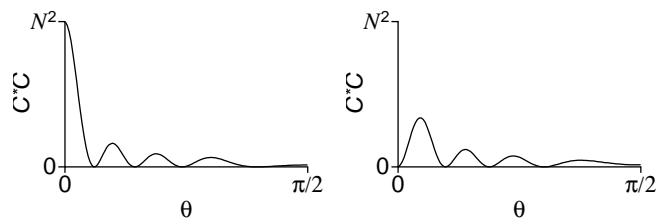


FIG. 2: Plots of the function  $\mathcal{C}^* \mathcal{C}$ . Notice the influence of  $l$  on the graph. Here  $l = 0$  (left) and  $l = \pm 1$  (right).

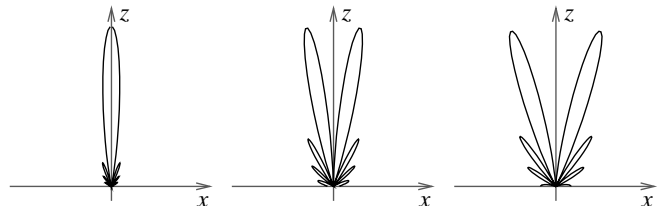


FIG. 3: Radiation patterns for radio beams generated by a circular antenna array with radius  $2\lambda$ ; all antennas are directly over ground. Without ground the electromagnetic waves would also be emitted symmetrically into the lower half space. The patterns are for  $l = 0$  (left),  $l = \pm 1$  (middle), and  $l = \pm 2$  (right).

on the  $z$  axis. If the topological charge is non-zero,  $l \neq 0$ , the fields of the beam cancel on the  $z$  axis resulting in a doughnut shaped beam profile that becomes wider for larger absolute values of the topological charge.

The Poynting vector is proportional to the energy density and points from the antenna array radially outwards,  $\mathbf{p}_{\text{far}} = \frac{\hat{\mathbf{r}}}{c} w_{\text{far}}$ . Therefore, the radiation pattern of the linear momentum is identical to that of the energy.

Radiation patterns of the orbital and spin angular momentum are displayed in Figs. 4 and 5, respectively. The orbital angular momentum density always points in the direction of  $-\hat{\theta}l$ , whereas the spin angular momentum changes its sign from cone to cone. Hence, the directions of the spin angular momentum density vectors alternate between  $-\hat{\theta}h$  and  $+\hat{\theta}h$ .

Often, spin is identified with polarization. I emphasize that this is not allowed for the spin angular momentum *density*; only the total spin angular momentum can be identified with polarization. For instance, taking  $l = 0$  and  $h = 1$ , the spin angular momentum density vanishes on the  $z$  axis, see Fig. 5 (left), whereas the electric and magnetic fields are maximal on the  $z$  axis and are right-hand circular polarized.

## VII. FLUXES

The total fluxes of energy, linear momentum, orbital and spin angular momentum follow from integrating the densities. Let  $S$  be a closed surface with the antenna array in its inside. The total fluxes through the surface are  $\frac{dW}{dt} = \int_S w_{\text{far}} c r^2 d\Omega$ ,  $\frac{d\mathbf{P}}{dt} = \int_S \mathbf{p}_{\text{far}} c r^2 d\Omega$ ,  $\frac{d\mathbf{L}}{dt} =$

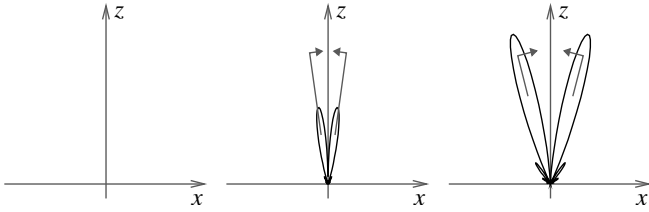


FIG. 4: Radiation patterns for the orbital angular momentum. The direction of the orbital angular momentum density vectors is in the direction of  $-\hat{\theta}l$  as displayed by the arrows  $\vec{r}$  and  $\hat{\phi}$ . The patterns are for  $l = 0$  (left),  $l = 1$  (middle), and  $l = 2$  (right).

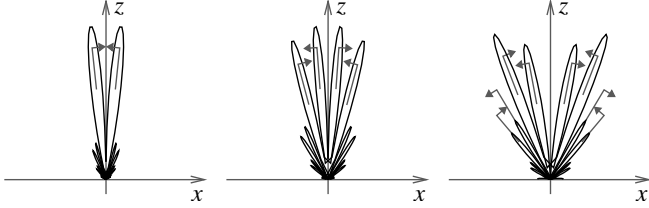


FIG. 5: Radiation patterns for the spin angular momentum. The directions of the spin angular momentum density vectors alternate between  $-\hat{\theta}h$  and  $+\hat{\theta}h$  as displayed by the arrows  $\vec{r}$  and  $\hat{\phi}$ . The patterns are for positive helicity,  $h = +1$ , and topological charge  $l = 0$  (left),  $l = \pm 1$  (middle), and  $l = \pm 2$  (right).

$\int_S \mathbf{l}_{\text{far}} cr^2 d\Omega$ , and  $\frac{d\mathbf{S}}{dt} = \int_S \mathbf{s}_{\text{far}} cr^2 d\Omega$ . Because of the rotation symmetry around the  $z$  axis, the orbital and spin angular momenta,  $\mathbf{L}$  and  $\mathbf{S}$ , are parallel to the  $z$  axis. The linear momentum is radiated symmetrically in the positive and negative  $z$  direction, thus the net vanishes,  $\mathbf{P} = 0$ , and the angular momentum of electromagnetic waves becomes an intrinsic, but non-local property.

Expressing the orbital and spin angular momentum in multiples of the total energy results in [2, 20]

$$\frac{L_z}{W} = \frac{dL_z/dt}{dW/dt} = \frac{l}{\omega} \quad (21)$$

and

$$\frac{S_z}{W} = \frac{dS_z/dt}{dW/dt} = \frac{h}{\omega}. \quad (22)$$

### VIII. DETECTING THE TORQUE

The torque of the angular momentum flux can be measured with an absorber that surrounds the antenna array in the upper half space, see Fig. 6. If the antenna array is directly over ground with reflectivity  $\rho_g = \frac{I_{\text{refl}}}{I_{\text{in}}}$ , and if the absorber has a reflectivity of  $\rho_a$  and a transmittance of  $T_a = \frac{I_{\text{trans}}}{I_{\text{in}}}$ , the torque is

$$\frac{dJ_z}{dt} = \alpha \frac{l+h}{\omega} \frac{dW}{dt}, \quad (23)$$

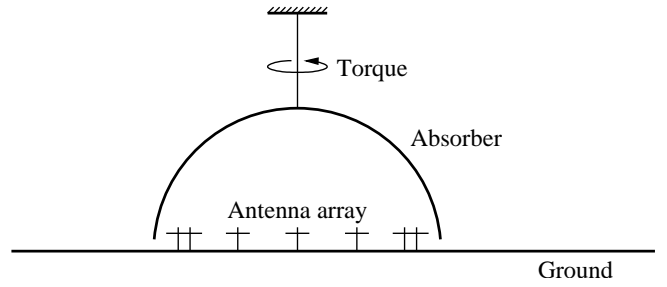


FIG. 6: A radio experiment that measures the torque of the total angular momentum flux.

where  $\frac{dW}{dt}$  is the power that is radiated by the antenna array and  $\alpha$  is determined by the reflectivities and the transmittance  $\alpha = \frac{1+\rho_g}{2}(1-T_a-\rho_a)\frac{1}{1-\rho_a}$ .

### IX. SPIN AND ORBITAL ANGULAR MOMENTUM OF A POINT DIPOLE

In section V it was demonstrated that the angular momentum of electromagnetic waves can be clearly separated into spin and orbital angular momentum, in agreement with the findings of S. M. Barnett [20]. However, Barnett is cautious in his conclusions, since it was unclear how to separate the angular momentum associated with a point dipole whose complex dipole moment reads  $\vec{\mu}(t) = \vec{\mu}e^{-i\omega t}$ . Here, I show that the separation into spin and orbital angular momentum is also clear for the dipole.

The vector potential of the point dipole reads

$$\mathbf{A}(\mathbf{r}, t) = \frac{i\mu_0\omega}{4\pi} \frac{\vec{\mu}(t)e^{ikr}}{r} \quad \text{with} \quad \vec{\mu} = \begin{pmatrix} \mu_x \\ \mu_y \\ 0 \end{pmatrix}. \quad (24)$$

Since the vector potential is identical to that of a small crossed electric dipole antenna which is fed with the complex current  $\mathbf{I}(t) = -i\frac{2\omega}{d}\vec{\mu}(t)$ , the above analysis can be applied. Decomposing the complex dipole,  $\vec{\mu} = \vec{\mu}^+ + \vec{\mu}^-$ , into one with positive and one with negative helicity,

$$\vec{\mu}^+ = \frac{1}{\sqrt{2}} \begin{pmatrix} 1 \\ i \\ 0 \end{pmatrix} \frac{\mu_x - i\mu_y}{\sqrt{2}} \quad (25)$$

and

$$\vec{\mu}^- = \frac{1}{\sqrt{2}} \begin{pmatrix} 1 \\ -i \\ 0 \end{pmatrix} \frac{\mu_x + i\mu_y}{\sqrt{2}}, \quad (26)$$

respectively, results in the spin angular momentum

$$\frac{S_z}{W} = \frac{1}{\omega} \frac{|\vec{\mu}^+|^2}{|\vec{\mu}|^2} - \frac{1}{\omega} \frac{|\vec{\mu}^-|^2}{|\vec{\mu}|^2} = \frac{1}{\omega} i(\mu_x\mu_y^* - \mu_y\mu_x^*)/|\vec{\mu}|^2. \quad (27)$$

Since no vorticity is present, the orbital angular momentum vanishes,  $L_z = 0$ . This rejects a suggestion [23] according to which half of the angular momentum should be attributed to spin and half to an orbital part.

That no vorticity is present can be seen if the point dipole is expressed by a circular array of dipoles in the limit of vanishing array radius. Only in the absence of vorticity, the circular array coincides with the point dipole in the limit  $R \rightarrow 0$ , otherwise the fields annihilate by destructive interference.

## X. RADIO WAVES ASSOCIATED WITH LONGITUDINAL CURRENTS

Since we have all learned that electromagnetic waves are transversal, it may sound strange to consider radio waves associated with longitudinal currents. Moreover, to my best knowledge, such waves have never been employed until recently [24]. However, as I present here, it is possible generate them.

Replacing the transversal crossed dipoles of the circular antenna array by electric dipoles that point in the longitudinal direction and feeding the longitudinal dipole antennas with the currents

$$\mathbf{I}_n = \frac{1}{\sqrt{2}} \begin{pmatrix} 0 \\ 0 \\ 1 \end{pmatrix} e^{2\pi i l \frac{\alpha}{N}}, \quad n = 1 \dots N, \quad (28)$$

the vector potential reads

$$\mathbf{A} = \frac{1}{\sqrt{2}} \begin{pmatrix} 0 \\ 0 \\ 1 \end{pmatrix} \mathcal{A}(r)\mathcal{C}(\theta, \phi) \quad (29)$$

where  $\mathcal{A}$  and  $\mathcal{C}$  are as given in section II.

Evaluating the densities of energy, linear momentum, and angular momentum yields

$$w_{\text{far}}^{\text{l}} = \frac{k^2}{4\mu_0} \left( \frac{I\mu_0 d}{8\pi r} \right)^2 (1 - \cos^2 \theta) (\mathcal{C}^* \mathcal{C}), \quad (30)$$

$$\mathbf{p}_{\text{far}}^{\text{l}} = \frac{\hat{\mathbf{r}} k^2}{4c\mu_0} \left( \frac{I\mu_0 d}{8\pi r} \right)^2 (1 - \cos^2 \theta) (\mathcal{C}^* \mathcal{C}), \quad (31)$$

and

$$\mathbf{j}_{\text{far}}^{\text{l}} = l \frac{-\hat{\theta} k^2}{4\omega\mu_0} \left( \frac{I\mu_0 d}{8\pi r} \right)^2 \left( \frac{1 - \cos^2 \theta}{\sin \theta} \right) (\mathcal{C}^* \mathcal{C}). \quad (32)$$

It is worth to compare these densities with those given in section IV, Eqs. (15)–(17). The essential difference is in the angular momentum density. For pure longitudinal currents, there is only an orbital part,  $\mathbf{j}_{\text{far}}^{\text{l}} = \mathbf{l}_{\text{far}}^{\text{l}}$ , and the spin part vanishes,  $\mathbf{s}_{\text{far}}^{\text{l}} = 0$ . This shows that electromagnetic waves associated with pure longitudinal currents can carry orbital, but no spin angular momentum.

Because of the term  $(1 - \cos^2 \theta)$  the beams of electromagnetic waves associated with longitudinal currents

have a deep null along their axis of propagation which gives rise to a doughnut shaped beam profile, even in the absence of any topological charge.

Radio waves associated with longitudinal currents are happy news for the LOIS team [25]. Their radio telescope which is currently under construction is the only device that employs 3D vector sensing antennas and is readily able to detect these waves. Other radio telescopes, e.g. LOFAR [26] and SKA [27], might be extended by adding vertical antennas in order to achieve the same capability.

## XI. GENERALIZING THE RESULTS

From the previous sections one might get the impression that the analysis is specific to radio waves emitted by a circular antenna array. However, as I show here, the analysis is more general and device independent.

Any device or source that generates a current distribution on a circle

$$\mathbf{I}(\rho, \Phi, z) = \frac{1}{2} \frac{N}{2\pi R} \frac{1}{\sqrt{2}} \begin{pmatrix} I \\ ihI \\ 0 \end{pmatrix} e^{i l \Phi} \delta(\rho - R) \delta(z), \quad (33)$$

where  $\rho, \Phi, z$  are cylindrical coordinates, results in the vector potential

$$\mathbf{A} = \frac{1}{\sqrt{2}} \begin{pmatrix} 1 \\ ih \\ 0 \end{pmatrix} \mathcal{A}(r)\mathcal{C}(\theta, \phi) \quad (34)$$

with  $\mathcal{C} = \frac{N}{2\pi} \int d\Phi e^{i l \Phi} e^{-i k R \sin \theta \cos(\Phi - \phi)}$  and  $\mathcal{A} = -\frac{I\mu_0 d}{8\pi} \frac{e^{i k r}}{r}$ , cf. Eqs. (3)–(4). Hence, for the current distribution given here, the results presented in the previous sections are valid without approximation.

Since the angular dependence of the vector potential can be expressed by its residuum, Eq. (5), there is no need that the current distribution is on the circle. The current distribution can be along any line that surrounds the origin. Moreover, the current distribution can be chosen arbitrarily in the  $x$ - $y$ -plane, provided the residuum keeps unchanged. Even if the residuum changes, all results presented above keep unchanged except of Figs. 2–5.

If the current distribution is not in a plane, but in three dimensional space, the situation becomes more complicated and will be presented elsewhere.

## XII. INTERFERENCES BETWEEN WAVES ASSOCIATED WITH TRANSVERSAL AND LONGITUDINAL CURRENTS

If the vector potential reads

$$\mathbf{A} = \frac{1}{\sqrt{2}} \begin{pmatrix} \alpha \\ \alpha i h \\ \beta \end{pmatrix} \mathcal{A}(r)\mathcal{C}(\theta, \phi), \quad (35)$$

the densities of energy and momenta are

$$w_{\text{far}} = |\alpha|^2 w_{\text{far}}^t + |\beta|^2 w_{\text{far}}^l - 2|\alpha\beta|w_{\text{far}}^i, \quad (36)$$

$$\mathbf{p}_{\text{far}} = |\alpha|^2 \mathbf{p}_{\text{far}}^t + |\beta|^2 \mathbf{p}_{\text{far}}^l - 2|\alpha\beta|\mathbf{p}_{\text{far}}^i, \quad (37)$$

$$\mathbf{l}_{\text{far}} = |\alpha|^2 \mathbf{l}_{\text{far}}^t + |\beta|^2 \mathbf{l}_{\text{far}}^l - 2|\alpha\beta|\mathbf{l}_{\text{far}}^i, \quad (38)$$

$$\mathbf{s}_{\text{far}} = |\alpha|^2 \mathbf{s}_{\text{far}}^t + |\beta|^2 \mathbf{s}_{\text{far}}^l - 2|\alpha\beta|\mathbf{s}_{\text{far}}^i. \quad (39)$$

The contributions associated with transversal currents are here denoted with the upper index ‘‘t’’ and are given in sections IV and V, Eqs. (15)–(19). The contributions associated with longitudinal currents are given in section X, and the contributions due to interferences read

$$w_{\text{far}}^i = \frac{k^2}{4\mu_0} \left( \frac{I\mu_0 d}{8\pi r} \right)^2 \sin\theta \cos\theta (\mathcal{C}^* \mathcal{C}) \cos(h\phi + \arg\beta^* \alpha), \quad (40)$$

$$\mathbf{p}_{\text{far}}^i = \frac{\hat{\mathbf{r}}k^2}{4c\mu_0} \left( \frac{I\mu_0 d}{8\pi r} \right)^2 \sin\theta \cos\theta (\mathcal{C}^* \mathcal{C}) \cos(h\phi + \arg\beta^* \alpha), \quad (41)$$

$$\mathbf{l}_{\text{far}}^i = l \frac{-\hat{\theta}k^2}{4\omega\mu_0} \left( \frac{I\mu_0 d}{8\pi r} \right)^2 \cos\theta (\mathcal{C}^* \mathcal{C}) \cos(h\phi + \arg\beta^* \alpha), \quad (42)$$

and

$$\begin{aligned} \mathbf{s}_{\text{far}}^i = & h \frac{-\hat{\theta}k^2}{4\omega\mu_0} \left( \frac{I\mu_0 d}{8\pi r} \right)^2 \left\{ -\cos\theta (\mathcal{C}^* \mathcal{C}) \right. \\ & \left. + \frac{1}{2} \sin\theta \frac{\partial}{\partial\theta} (\mathcal{C}^* \mathcal{C}) \right\} \cos(h\phi + \arg\beta^* \alpha) \\ & + \frac{-\hat{\phi}k^2}{4\omega\mu_0} \left( \frac{I\mu_0 d}{8\pi r} \right)^2 (\mathcal{C}^* \mathcal{C}) \sin(h\phi + \arg\beta^* \alpha). \end{aligned} \quad (43)$$

If integrated, most of the interferences vanish. This allows to carry over the principle of superposition of electromagnetic waves to their mechanical properties,

$$W = |\alpha|^2 W^t + |\beta|^2 W^l, \quad (44)$$

$$\mathbf{P} = |\alpha|^2 \mathbf{P}^t + |\beta|^2 \mathbf{P}^l, \quad (45)$$

$$L_z = |\alpha|^2 L_z^t + |\beta|^2 L_z^l, \quad (46)$$

$$S_z = |\alpha|^2 S_z^t, \quad S_z^l = 0. \quad (47)$$

However, for some quantities the interferences do not cancel

$$L_x^i \neq 0, \quad L_y^i \neq 0, \quad S_x^i \neq 0, \quad S_y^i \neq 0, \quad (48)$$

and further investigations are required to figure out when and why the mechanical properties of electromagnetic waves can be linearly added. Knowledge of the latter would greatly simplify future analysis of electromagnetic waves associated with general three dimensional current distributions.

### XIII. DISCRETE SOURCES AND THE UNCERTAINTY PRINCIPLE

If the sources are continuous like in section XI, the analysis is exact and the number of orbital angular momentum states is unbounded. In contrast, if the sources are discrete, the presented analysis is an approximation. Luckily, the approximation improves very fast with the number of discrete sources; and there is typically no need to worry about the accuracy.

However, if only very few discrete sources are present or if one is interested in the number of orbital angular momentum states that can be utilized, an alternative approach becomes favorable. The alternative approach starts from a continuous source distribution and the discrete nature of the sources enters via imposing a Pac-Man mask that has slits at the appropriate positions. Due to Fourier convolution with the mask, the uncertainty principle enters and gives rise to a distribution in the orbital angular momentum [28]. This distribution has a periodicity of  $N$  and peaks of width proportional to  $1/N$ . This limits the number of orbital angular momentum states that can be utilized in a circular array of  $N$  equidistributed discrete sources to  $\#\{l\} \leq N - O(1/N)$ , where the implied constant in the last term depends on the noise level and on the details of the discrete sources.

### XIV. SUMMARY

A simple and concise analysis of twisted radio waves was given which highlights profound aspects of spin and orbital angular momentum, analytically. Namely, how twisted radio waves are connected to helicity and vorticity; that the angular momentum of radio waves is an intrinsic property; that it is transported all the way out to infinity; that it can be clearly separated into spin and orbital angular momentum; and that spin unlike its density can be identified with polarization.

In particular, separating the angular momentum into spin and orbital angular momentum, I find that the density of orbital angular momentum depends on the vorticity only and can be expressed by quite simple terms, whereas the density of spin angular momentum depends on both, helicity and vorticity.

The approach via an antenna array illuminates light from a new perspective and complements previous studies of orbital angular momentum of electromagnetic waves [2, 20, 21]. In particular, as a special case of the present approach, it is now for the first time possible to separate the angular momentum of an electric point dipole [29] into its spin and its orbital part.

Emerging as a byproduct, but being of deep interest in its own is the finding in section X. Radio waves associated with longitudinal currents have never been investigated until recently, nor their existence has even been appreciated. It is tempting to speculate whether the universe is densely filled with such waves opening a new

window for astronomical observations.

### Acknowledgment

My warmest thanks are due to Professor Bo Thidé, Dr. Jan Bergman and Dr. Tobia Carozzi for valuable dis-

cussions. Part of the work was supported by the Centre for Dynamical Processes and Structure Formation, Uppsala University, Sweden.

- 
- [1] J. H. Poynting, Proc. R. Soc. A **82**, 560 (1909).
- [2] L. Allen, M. W. Beijersbergen, R. J. C. Spreeuw, and J. P. Woerdman, Phys. Rev. A **45**, 8185 (1992).
- [3] S. Franke-Arnold, L. Allen, and M. Padgett, Laser & Photonics Reviews **2**, 299 (2008).
- [4] C. N. Cohen-Tannoudji, Rev. Mod. Phys. **70**, 707 (1998).
- [5] K. Ladavac and D. Grier, Opt. Express **12**, 1144 (2004).
- [6] M. Harwit, Astrophys. J. **597**, 1266 (2003).
- [7] G. Gibson et al., Opt. Express **12**, 5448 (2004).
- [8] A. Mair, A. Vaziri, G. Weihs, and A. Zeilinger, Nature **412**, 313 (2001).
- [9] A. Vaziri, G. Weihs, and A. Zeilinger, Phys. Rev. Lett. **89**, 240401 (2002).
- [10] B. Thidé et al., Phys. Rev. Lett. **99**, 087701 (2007).
- [11] O. Stål et al., Phys. Rev. Lett. **98**, 071103 (2007).
- [12] S. Panda, S. Mohanty, J. Padmanabhan, and O. Stål, JCAP **11**, 22 (2007).
- [13] Y. N. Istomin, Phys. Lett. A **299**, 248 (2002).
- [14] C. Paterson, Phys. Rev. Lett. **94**, 153901 (2005).
- [15] B. Thidé et al., Phys. Rev. Lett. **95**, 255002 (2005).
- [16] B. Thidé, in *Mathematical Modelling of Wave Phenomena*, edited by B. Nilsson and L. Fisherman (Växjö University Press, Växjö, Sweden, 2004), pp. 315–331.
- [17] M. V. Khotyaintsev, V. N. Mel'nik, B. Thidé, and O. O. Konovalenko, Sol. Phys. **234**, 169 (2006).
- [18] J. M. Jauch and F. Rohrlich, *The Theory of Photons and Electrons*, (Addison-Wesley, Cambridge, 1955).
- [19] K. Gottfried, *Quantum Mechanics*, (Benjamin, New York, 1966).
- [20] S. M. Barnett, J. Opt. B **4**, S7 (2002).
- [21] L. Allen, M. J. Padgett, and M. Babiker, Prog. Opt. **39**, 291 (1999).
- [22] J. D. Jackson, *Classical Electrodynamics* (Third Edition, John Wiley & Sons, New York, 1998).
- [23] J. H. Crichton, and P. L. Marston, *Electron. J. Diff. Eqns. Conf.* **4**, 37 (2000).
- [24] T. D. Carozzi, *Polarimetry and angular momentum detection with the Square Kilometre Array (SKA)*, presentation at the *7th LOIS Workshop* (Växjö, Sweden, June 17, 2008), <http://www.lois-space.net/Workshops/-Vaxjo080616-18/Presentations/carozzi.pdf>
- [25] <http://www.lois-space.net/>
- [26] <http://www.lofar.org/>
- [27] <http://www.skatelescope.org/>
- [28] S. Franke-Arnold et al., New J. Phys. **6**, 103 (2004).
- [29] M. Abraham, Physik. Zeitschr. **XV**, 914 (1914).